University of South Carolina
Scholar Commons

2017

An Application of Dempster-Shafer Fusion Theory to Lithium-ion Battery Prognostics and Health Management

John Weddington
University of South Carolina

An Application of Dempster-Shafer Fusion Theory to Lithium-ion Battery Prognostics and Health Management

by

John Weddington

Bachelor of Science
The Citadel, The Military College of South Carolina 2011

_____

Submitted in Partial Fulfillment of the Requirements

for the Degree of Master of Science in

Electrical Engineering

College of Engineering and Computing

University of South Carolina

2017

Accepted by:

Bin Zhang, Director of Thesis

Xiaofeng Wang, Reader

Cheryl L. Addy, Vice Provost and Dean of the Graduate School

ACKNOWLEDGMENTS

My Lord, Jesus, I need not say much except that you have seen me through, immeasurably. Every time I hit a wrong turn, you filled me with wisdom to overcome every obstacle. Thank you for your patience with me as I have sought to achieve this in my own strength forgetting to rely on you. Thank you for giving me friends, family, professors, bosses, and coworkers who has been so incredibly supportive. You have blessed me in more ways than I can count.

Elizabeth, Hannah, and Lillian, my beautiful wife and daughters. What can I say that would summarize how meaningful your support has been to me over these years. I cannot thank you enough for being a bedrock of warmth and encouragement over the many long months and late nights. I have missed family dinners, bedtime stories, dance parties, and vacations to achieve this. All the while you have remained committed to helping me complete my coursework and thesis, and you have been selfless in doing so. However, our marriage has deepened and our famliy is stronger than ever as we have learned to set priorities and make our time count. I look forward to having my life back with you!

My parents for teaching me perseverance in the face of tremendous obstacles. Working full time with a young family, and pursuing graduate school has certainly characterized an obstacle.

Dr. Zhang, thank you for all of your patience. Working with me remotely much of the time has been a chore I am sure, but I am thankful to you for helping me achieve this goal. Without your encouragement, I would not have been able to see this through to completion. My family and I thoroughly enjoyed being welcomed

ABSTRACT

Prognostics and Health Management (PHM) is the discipline involving diagnostics and prognostics of components or systems, with the primary objective of increasing the overall reliability and safety of these components or systems. PHM systems convert raw sensor data into features, and utilize state observers to estimate the current damage state online. Popular state observers are the traditional Kalman filter, along with its non-linear extensions, and the particle filter. Each technique has differing advantages. This thesis investigates the fusion of results from different techniques in order to achieve a more trustworthy probability of detection (PoD) during diagnosis and a more reliable remaining useful life (RUL) prediction in prognosis. Models for extended Kalman filter (EKF) and particle filter (PF) are developed from the feature data. The results from EKF and PF are then fused using an application of Dempster-Shafer theory (DST). Different models are utilized for EKF and PF in order introduce multi-model PHM, and to optimize the performance of each technique for both aging detection and RUL prediction. Prognostics is triggered when one-step-ahead predictions compared against the healthy battery demonstrate aging. DST is then applied to the prognostic results from EKF and PF. The result of DST is a density function whose performance can be compared with that of EKF and PF. DST allows for the fusion of multiple sensors and state estimates.

TABLE OF CONTENTS

LIST OF TABLES

LIST OF FIGURES

CHAPTER 1

INTRODUCTION

1.1 MOTIVATION

Batteries are temporary power sources with limited lifespan. Over time, they experience degraded performance as a result of normal use, as well as accelerated degradation under strained operating conditions. Rechargeable batteries are utilized in a wide number of critical applications. In particular, lithium-ion (Li-ion) batteries are growing in popularity over traditional technologies such as nickel-cadmium (NiCd) and nickel-metal hydride (NiMH). Beginning around 2000, Li-ion battery production began to grow, and has since expanded such that Li-ion batteries make up more than 60% of all rechargeable batteries produced [1, 2]. Roughly 40% of mined lithium metal is used for Li-ion battery production. This trend underlines the the importance of studying the effects of failure of Li-ion battery systems in particular. Consumer-grade devices such as smartphones and tablets, pacemakers for the medical field, industrial battery-powered wireless transmitters used in remote instrumentation applications, as well as electric vehicles used in military and aerospace applications all depend upon the reliable performance of Li-ion battery systems for continued operation.

Prognostics and health management (PHM) is a discipline which involves the management of components and systems such that catastrophic failures are avoided through early detection and prediction of the end of life (EoL). Within PHM, major components enabling techniques include dignostics and prognostics. Diagnostics is described in three phases: (1) detection of anomalies or failure incipience, (2)

identification (or isolation) of the fault mode, and (3) estimation of the severity of the fault. Prognostics involves projection of the fault into the future, and calcluation of remaining useful life (RUL) or time to failure (TTF), where TTF describes the absolute time until the EoL, and the RUL takes into account the amount of time needed to take corrective action.

Once implemented, PHM systems are intended to influence decision-making. This could involve reconfiguration for control applicaitons, or maintenance planning. Whatever, the case, there is risk associated with inaccuracy. For these techniques to be of any use, they must provide accurate and reliable estimates of the actual state of the Li-ion battery system, which assumes that the uncertainty in the estimate is properly managed. The focus of this thesis is to present a method for managing the uncertainty in PHM systems through the use of data fusion techniques. The purpose of fusing any two or more sets of information is to increase the reliability of the meausrement. In our case, the measurement is more reliable if it accurately represents the probability of fault detection, and produces a bounded TTF prediction whose bounds become tighter as time progresses.

1.2 CONTRIBUTIONS

develop a multi-mode applicaiton develop a DS-based fusion approach Extend DS fusion to include two types of uncertainties verification on a set of li-ion batteries

1.3 ORGANIZATION

This remaining text in organized in the following manner. Section **??** provides .... e remaining sections detail the theoretical basis, and apply this theory to a Li-ion battery PHM application.

CHAPTER 2

LITERATURE REVIEW

In order to begin either diagnostics or prognostics, an accurate estimate of the current health must be available. State-of-charge (SOC) is a common metric used in many deployed battery management systems, especially consumer-grade batteries, which defines the remaining charge before the voltage is depleted. This is useful in the short term, but does not answer the question as to how many discharge-recharge cycles will this battery be able to withstand before needing to be replaced. The state-of-health (SOH) of the battery meets this requirement. SOH is an indirect metric attained by extracting the feature from direct measurement data. It represents the remaining capacity of the Li-ion battery, measured in Amp-hours (Ah). Critical systems designed for long-term reliability cannot depend solely on the SOC of their Li-ion systems, so the SOH must be considered. This work does not detail different methods of extracting the SOH, as that is application-dependent.

Once the SOH feature has been extracted, it needs to be placed within a framework that is compatible with diagnosis. Typically this involves the use of algorithms to predict one-step ahead (to achieve *priori* state estimation) and then corrected with measurement (to achieve *posteriori* state estimation), which is useful in diagnosis. This *posteriori* state estimation can then be utilized as an initial condition for long term prediction in prognosis.

On-board Li-ion battery detection involves the use of state estimation techniques [3, 4]. In the framework of Bayesian theory, a state estimator is used to make a one-step prediction of the current battery capacity, which is then filtered when the

new measurement becomes available to obtain the *posteriori* capacity distribution. The *posteriori* distribution is then compared with a baseline distribution (established from the data from the healthy system) to calculate the probability of detection in terms of battery capacity degradation. In the past few decades, a number of different state estimators were developed including wavelet analysis [5], Kalman filter (KF) [6], multiple model adaptive estimation [7, 8], extended Kalman filter (EKF) [9], particle filter (PF) [10–12], and autoregressive integrated moving average [13, 14].

With the *posteriori* distribution of battery capacity, prognosis is executed to estimate the time to failure, measured by number of charge-discharge cycles. Each estimator differs from the other by offering better performance in different aspects. For example, the EKF is founded upon the efficient, optimal KF, which is able to accurately produce the underlying state for linear systems. The PF is a complex sampling algorithm that discovers the underlying state by means of sequential Monte-Carlo calculations, but it is well-suited for nonlinear and non-Gaussian systems. In order to utilize the best from each algorithm, it is desirable to fuse their results. As uncertainty is a major consideration in real world applications, the fusion must take uncertainty into consideration.

Fusing prognostic results is an important concept in literature. An adaptive neuro-fuzzy inference system (ANFIS) is developed to fuse data for RUL prediction in [15]. A kernel-based regression algorithm is presented in [16]. In [17], a fusion prognostics method is proposed to fuse results from a physics of failure model and data driven model using results from a failure modes, mechanisms, and effects analysis (FMMEA). Support vector data description is utilized to fuse multiple health indicators for enhancing gearbox fault diagnosis and prognosis [18].

A thorough review of data fusion is given in [19]. For the purposes of this work, we focus on decision fusion, which is the process of combining the reasoning from different algorithms to enable a decision to be made. These features are then fused, and the

results are classified into decision categories. There are four prevalent methods for decision fusion: voting logic, abductive reasoning (fuzzy logic inference), probability theory (Bayesian fusion), and belief theory (DST-based fusion).

Voting fusion is used heavily in industry with redundant instrumentation. Typical methods for voting fusion are threshold, majority, median, and others [20]. Voting fusion is mostly used with crisp numbers, but its application has expanded into numerous domains, including dependable system design with unreliable components.

Fuzzy logic inference expands voting into the domain of "gradual decision making" [21]. Fuzzy logic is also called soft voting, because the fusion rules are not crisp, but allow for many different scenarios. The task of fusion using fuzzy methods was demonstrated in [22]. Depending upon the complexity of the problem, fuzzy logic may require extensive understanding of system dynamics to perform effectively.

Bayesian theory is based on probability theory or Bayes' theorem. The theory relates evidence and belief using prior and current information. Being a proven method, it maintains a larger contingent of supported applications of the theory. This is due, in part, to its simple formulation, which enables it to be better understood than other proposed methods [23].

Dempster-Shafer Theory (DST) builds upon Bayesian probability theory by incorporating unknowns and confidence measures into its calculations, and is typically categorized under the heading "Belief Theory" or "Evidence Theory" [24]. DST has definite advantages over the Bayesian method under certain circumstances, primarily in its ability to explicitly consider unknowns when combining evidence [25, 26]. It is based on the concept of assigning a degree of belief or confidence to certain propositions on the basis of combining all the available evidence.

Many different applications of DST have been implemented. Gas turbine engine test cell sensor validation was improved with the use of DST [27]. A DST-based neural network (DSETNN) was proposd in [28], in order to address problems associated with

constructing basic belief assignments (bba's), as well as the issue of dependence among information sources. Smets proposed the Transferrable Belief Model (TBM) as an extension to DST which separates decision from belief, by breaking the belief model into two levels: credal and pignistic [29, 30]. DST was applied to regression [31], and later to machinery prognostics [32]. In general, however, most of existing works are fusion of diagnostic results and the application of DST in prognostics is largely still an open problem.

To address this problem, the research in this work extends the DST fusion to prognostics to achieve better estimation of RUL. Note that the use of Dempster-Shafer theory (DST) to fuse diagnostic results in Li-ion batteries was originally treated in [33]. In the proposed fusion of prognosis, only reasonable estimates of the uncertainty are needed to implement DST fusion. Once the uncertainty associated with RUL predictions from EKF and PF are explicitly defined and isolated, DST-fusion can consider the unique contribution each type of uncertainty makes to the RUL when combining the predictions. This work introduces a novel method for generating an RUL distribution. By buliding upon the strong theoretical background of DST, the proposed RUL distribution is able to be generated with relative ease, and with computational efficiency. The other applications of DST in prognostics have focused on regression, which involves expensive computations. However by focusing strictly on developing an RUL distribution, computational efficiency is preserved.

CHAPTER 3

APPROACH DEVELOPMENT

This section details a method for aging detection (AD) and prognosis of Li-ion batteries by combining the EKF and the PF to manage the uncertainty inherent in each state estimator. Figure 3.1 demonstrates the flow chart used in designing the proposed prognostic system. In our application, we have implemented different models for EKF and PF, thus demonstrating that our DST fusion technique can be implemented indepent from state estimation technique and underlying model. Instead, DST fusion is dependent upon accurate representations of uncertainty present within the different techniques. In our framework, we could conceivably fuse any two or more prognostic techniques simultaneously, only being constrained by the hardware processing capability (e.g. CPU clock speed, parallel computing, etc.). Thus DST is scalable as necessary to describe the complexities of the unit under test (UUT).

The nonlinear process model (from cycle $k-1$ to cycle k) for battery capacity degradation is described as a hidden Markov model (HMM) by

$$x_k = f(x_{k-1}, u_{k-1}) + w_{k-1} \tag{3.1}$$

where x_k and x_{k-1} are the battery capacity state at the current cycle, k, and the previous cycle, $k-1$, $f(\cdot)$ is a nonlinear model describing the battery capacity degradation, u_{k-1} is the operating condition, and w_{k-1} is process noise. The observation model is

$$z_k = h(x_k) + v_k \tag{3.2}$$

7
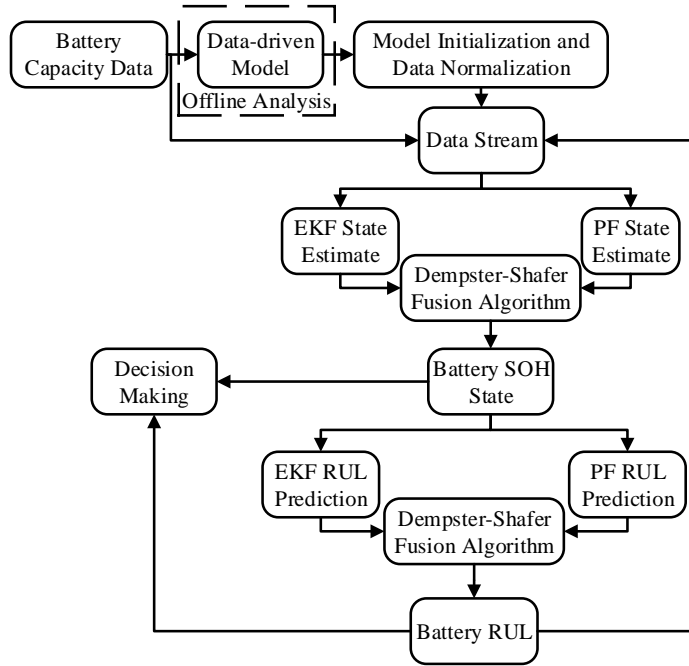
Figure 3.1   Fusion prognostics system diagram.

where z is the observation vector, which in battery capacity degradation application is the capacity calculated by Coulomb-counting, $h(\cdot)$ is a nonlinear observation function, and v_{k+1} is the measurement noise. Note that process noise ω and measurement v must be Gaussian in EKF while they can be any non-Gaussian noises in PF.

3.1   EXTENDED KALMAN FILTER

For state estimation, the KF is known as a linear quadratic optimal filter. This algorithm is a linear, discrete time, finite dimensional time-varying state estimator that minimizes the mean-squared error (MSE). Capacity degradation of Li-ion batteries is a nonlinear process, described with respect to charging-discharging cycles, for which KF is insufficient and necessitates the use of EKF. The EKF expands the KF to incorporate non-linear dynamics, by linearizing around the current state, as described by the mean and covariance. EKF is evaluated in two stages: prediction

8

and correction. Both the prediction and correction steps require the calculation of the partial derivatives (the Jacobian) of $f(\cdot)$ and $h(\cdot)$, which are used for local linearization, as shown below:

State Jacobian:

$$F_k = \frac{\partial f}{\partial x}\Big|_{\hat{x}_{k-1|k-1}, u_{k-1}} \tag{3.3}$$

Observation Jacobian:

$$H_k = \frac{\partial h}{\partial x}\Big|_{\hat{x}_{k-1|k-1}} \tag{3.4}$$

The prediction step of EKF comprises the following:

1. Project the *a priori* state at the next time instant (cycle for battery SOH application) by using the model

$$\hat{x}_{k|k-1} = f(\hat{x}_{k-1|k-1}, u_k) \tag{3.5}$$

2. Project the prediction error covariance, P, ahead

$$P_{k|k-1} = F_{k-1}P_{k-1|k-1}F_{k-1}^T + Q_{k-1} \tag{3.6}$$

where Q is the process noise covariance matrix.

For the correction step of EKF:

1. Compute the Kalman gain, K

$$K_k = P_{k|k-1}H_k^T \left(H_k P_{k|k-1} H_k^T + R_k\right) \tag{3.7}$$

2. Update error covariance, P

$$P_{k|k} = (I - K_k H_k)P_{k|k-1} \tag{3.8}$$

3. Update the state estimate with measurement

$$\hat{x}_{k|k} = \hat{x}_{k|k-1} + K_{k-1}\left(z_{k-1} - h(x_{k|k-1})\right) \tag{3.9}$$

The *posteriori* estimate provided by Eq. (3.9) provides initial condition for long-term prediction in RUL calculation. The state models are recursively used to generate the a priori estimation of battery capacity in all future cycles. These *a priori* battery capacity state distributions are compared against the battery capacity failure threshold to calculate the Time to Failure (TTF) or RUL distribution. Note that since no measurement available in this long-term prediction, the correction step cannot be implemented, which will result in increase of uncertainty described in P in 3.6. The uncertainty must be properly managed to achieve reliable prognosis.

3.2 PARTICLE FILTER

One disadvantage of the EKF is that the desired pdf is estimated by a Gaussian, and as the system under study is not normally distributed, the estimation could deviate from the actual distribution and diverge [12, 34, 35]. The PF is developed as a solution for nonlinear random non-Gaussian systems. The algorithm assumes the process state equations can be effectively modeled as a first-order nonlinear Markov process in Eqs. (3.1) and (3.2) . The state x and observation z for cycles 1 to k are defined as

$$x_{0:k} \triangleq \{x_0, x_1, \ldots, x_k\}, z_{1:k} \triangleq \{z_1, z_2, \ldots, z_k\} \tag{3.10}$$

The PF is also known as a sequential Monte Carlo method for state-space inference. PF is able to accommodate nonlinearities easily, provided enough particles are used. The particle filter aims to obtain a set of weighted particles to estimate the battery capacity based upon a nonlinear model. The algorithm begins with a set of N particles available at cycle $k-1$ that describe the battery capacity distribution, which is also the target distribution, denoted as $p(x_{0:k-1}|z_{1:k-1})$. The objective of filtering is to obtain a set of N new particles to approximate the target distribution at cycle k, π_k. To obtain these new particles, a known distribution is chosen by the user to be the proposal distribution. A set of N particles are sampled from the proposal distribution

q_k (also known as the importance distribution) as shown,

$$\{x_{0:k}^{(i)}\}_{i=1,\dots,N} \sim q_k(x_{0:k}^{(i)}) \tag{3.11}$$

and compared against the target distribution. The true distribution is approximated by a set of N weighted particles, $\{w_k^{(i)}, x_{0:k}^{(i)}\}_{i=1,\dots,N}$

$$\sum_{i=1}^{N} w_k^{(i)}\phi_k(x^{(i)}) \xrightarrow{N\to\infty} \int \phi_k(x_{0:k})\pi_k(x_{0:k})dx_k \tag{3.12}$$

where ϕ_k is any π_k integrable function and the sum of all weights is 1. To accommodate the difference between importance distribution and target distribution, importance sampling set the weights of N particles equal to the ratio between them, i.e.,

$$\tilde{w}(x_{0:k}^{(i)}) = \frac{\pi(x_{0:k}^{(i)})}{q_k(x_{0:k}^{(i)})} \tag{3.13}$$

which is normalized as

$$w(x_{0:k}^{(i)}) = \frac{\tilde{w}(x_{0:k}^{(i)})}{\sum \tilde{w}(x_{0:k}^{(i)})} \tag{3.14}$$

With this new set of weights, the target distribution can be approximated as:

$$\pi(x_{0:k}) = \sum_{i=1}^{N} w_k^{(i)}\delta(x_{0:k} - x_{0:k}^{(i)}) \tag{3.15}$$

In a simple case of the particle filter, Bootstrap filter, the importance density function is set as the *a priori* pdf,

$$q_k(x_{0:k}|x_{0:k-1}) = p(x_k|x_{k-1}) \tag{3.16}$$

In this setting, the weights for the newly generated particles are proportional to the likelihood of new observations, i.e.

$$w_k^{(i)} = w_{k-1}^{(i)} \cdot p(z_{1:k}|x_{0:k}^{(i)}) = w_{k-1}^{(i)} \cdot p(z_k|x_k^{(i)}) \tag{3.17}$$

In particle filters, degeneracy is a problem that must be addressed. Degeneracy can be described as the decreasing number of more heavily weighted particles as sampling

continues to be performed. This leads to a dominance of particles with small weights describing the distribution. In practice, this results in inaccurate estimation of the actual state. Degeneracy is addressed by resampling. Resampling effectively replaces the smaller-weighted particles with larger-weighted particles, so as to describe to true distribution with higher veracity [36]. Sequential Importance Resampling (SIR) is the PF implementation chosen for this application due to its robustness. The variance of the weighted particles generated by the Bootstrap filter is calculated using an effective sample size:

$$\tilde{N}_{eff} = \frac{1}{\sum_{i=1}^{N} (w_k^{(i)})^2} \tag{3.18}$$

When $\tilde{N}_{eff} < N_{threshold}$, the particles are resampled to eliminate particles with small weights. The steps in SIR are included in Algorithm 1.

Algorithm 1 Sequential Importance Resampling

1: $N^{(i)} = \left\lfloor N \cdot w_{k1}^{(i)} \right\rfloor$ ▷ Identify best particles

2: $\overline{N} = N - \sum N^{(i)}$ ▷ Resample $\overline{N}$ particles

3: $N_{res} = \frac{N \cdot w_k^{(i)} - N^{(i)}}{\overline{N}}$ ▷ Resampled particle weights

4: $S_{res} = \left\{ \sum_1^i N_{res}^{(i)} \right\}_{i=1,...,\overline{N}}$ ▷ Cumulative sum

5: $\{u^{(i)}\}_{i=1,...,\overline{N}} \sim \mathcal{U}[0,1]$ ▷ Sample from uniform distribution

6: $SORT$: $u^{(i)}$ $s.t.$ $u^{(i)} < u^{(i+1)}$ ▷ Ascending sequential order

7: **for** $i = 1 : \overline{N}$ **do**   ▷ Index $N^{(i)}$ with resampled particles

8:     **if** $u^{(i)} < S_{res}^{(i)}$ **then**

9:        $N^{(i)} = N^{(i)} + 1$

10:     **end if**

11: **end for**

12: $\left\{ x_{0:k-1}^{\left(i \cdot N^{(i)}\right)} \right\}_{i=1,...,N} \sim q_k \left(x_{0:k} | x_{0:k-1}^{(i)} \right)$ ▷ Resampling

---

3.3 DEMPSTER-SHAFER COMBINATION THEORY FOR FUSION

In DST, the concept of *belief variables* is introduced [37]. Each belief variable is characterized by its *basic belief assignment* (bba), m, which can be described as the confidence measure a source of information assigns to a specific hypothesis. If

$A_1, \ldots, A_n$ are the hypotheses, or sets, of interest where each $A_i \in 2^X$, then

$$m : 2^X \rightarrow [0,1], \quad \sum_{i=1}^{n} m(A_i) = 1, \quad m(\varnothing) = 0 \tag{3.19}$$

Using these bba's, "Dempster's Rule" is the fundamental equation governing the combination of evidence in belief theory [38].

$$(m_i \oplus m_j)(C) = \frac{\sum\limits_{A \cap B = C} m_i(A)m_j(B)}{1 - K}; \quad A \neq \varnothing \tag{3.20}$$

$$(m_i \oplus m_j)(\varnothing) = 0, \tag{3.21}$$

$$K = \sum_{A \cap B = \varnothing} m_i(A)m_j(B), \tag{3.22}$$

where m is the mass for each hypotheses, i and j are the sources of information, EKF and PF. C is the output, which is the battery capacity state in the fusion of diagnosis and battery RUL in the fusion of prognosis. A and B are hypotheses about the battery capacity and RUL: healthy or faulty. In our application, two other hypotheses are including to represent the uncertainty.

The sum of the masses in the numerator can be known as the *belief measure* of the hypothesis, which is also called the *support measure* in some literature. The denominator is called the *plausibility measure* [39]. The belief and the plausibility provide confidence bounds, which, when combined as indicated in Eq. (3.20), supply degrees of belief for the output. Equation (3.21) is the probability mass of the null set. K represents the mass associated with conflicting evidence. In Bayesian theory, the resulting probabilities are limited to distribution between the hypotheses, as in $P(A) = 1 - P(B)$. This assumes crisp separation of probabilities between the two hypotheses, which is not a safe assumption in critical systems. The flexibility of DST allows for more states to be defined easily. If for instance a Bayesian decision fusion system is required to utilize two sensors to discern whether a system is healthy or faulty, and the resulting probabilities are equally divided, the results can be confusing. This could imply a number of different scenarios, including improperly

defined hypotheses or innacurate sensor information. This level of uncertainty is not acceptable for online decision-making. DST is a quantitative means of representing uncertainty. In other words, DST allows for the explicit definition of alternative scenarios. These new proposed states can be various combinations of the original states. Shafer's overview of DST in [26] identified the important assumptions when approaching an appplication of DST:

1. the assigned masses are subjective in nature, not objective,

2. the sources are independent from one another,

3. the uncertainties within the problem are explicitly represented, and

4. the combination rule is carried out computationally.

The probability masses, as explained above, are not actual probabilities. These are expected to subjective masses from the perspective of the source. It follows then that DST will produce meaningless results if source i and source j are dependent upon one another, and are biased in the same manner. This means that DST cannot be used in cases of common uncertainty. If proposed states are in direct conflict with one another, which is mathematically represented by disjoint sets, DST produces a result of 0, per Eq. (3.21). In the event that sources deviate substantially from one another, DST will not produce confidence bounds. This is intuitive, since directly contradictory results cannot be combined by averaging or other methods.

Consider an example using our Li-ion battery system, Fig. 3.2. Notice that the state estimate pdfs from EKF and PF have no overlap. Considering three hypotheses, healthy, faulty, or uncertain states, the results from EKF and PF are directly contradictory. If the below combination rules are applied:

$$m(F) = \frac{m_{\mathrm{PF}}(F)m_{\mathrm{EKF}}(F) + m_{\mathrm{PF}}(F)m_{\mathrm{EKF}}(U) + m_{\mathrm{PF}}(U)m_{\mathrm{EKF}}(F)}{1 - (m_{\mathrm{PF}}(H)m_{\mathrm{EKF}}(F) + m_{\mathrm{PF}}(F)m_{\mathrm{EKF}}(H))}$$

$$m(U) = \frac{m_{\mathrm{PF}}(U)m_{\mathrm{EKF}}(U)}{1 - (m_{\mathrm{PF}}(H)m_{\mathrm{EKF}}(F) + m_{\mathrm{PF}}(F)m_{\mathrm{EKF}}(H))}$$

$$m(H) = 1 - (m(F) + m(U))$$

The results of fusion would be as follows:

$$m_{\text{EKF}}(F) = 1 \quad m_{\text{EKF}}(H) = 0 \quad m_{\text{EKF}}(U) = 0$$

$$m_{\text{PF}}(F) = 0 \quad m_{\text{PF}}(H) = 1 \quad m_{\text{PF}}(U) = 0$$

$$m(F) = 0 \quad m(H) = 1 \quad m(U) = 0$$

This result is counterintuitive. However, if a methodology for uncertainty could be incorporated into the measurement, the results would change drastically. By considering the variance inherent to EKF and PF as its uncertainty the results are as follows:

$$m_{\text{EKF}}(F) = 0.7 \quad m_{\text{EKF}}(H) = 0 \quad m_{\text{EKF}}(U) = 0.3$$

$$m_{\text{PF}}(F) = 0 \quad m_{\text{PF}}(H) = 0.75 \quad m_{\text{PF}}(U) = 0.25$$

$$m(F) = 0.4 \quad m(H) = 0.525 \quad m(U) = 0.075$$

These results are much improved. In the previous example, DST essentially ignores the EKF results, however, by incoporating a rudimentary method of uncertainty representation, the results are more intuitive. Since the PF has a slightly tighter variance, DST prodcues a result slightly favoring a healthy battery, but essentially demonstrates that there is not enough information to conclude a faulty battery. This result also demonstrates the need for more thorough uncertainty quantification.

However, many researchers have proposed extensions to DST in an effort to address the problem posed by strongly conflicting evidence, as presented in [40]. They claim that the normalization factor in Eq. (3.22) has the effect of entirely ignoring conflict, and attributing associated masses to the null set, Eq. (3.21). When the upper and lower bounds of DST are interpretted probabilistically, inaccurate and non-intuitive results are possible, as shown in [41, 42]. This is addressed by using a discounting function, which is mathematically more rigorous [25, 43]. This discounting function must account for the absolute reliability of the sources. In this
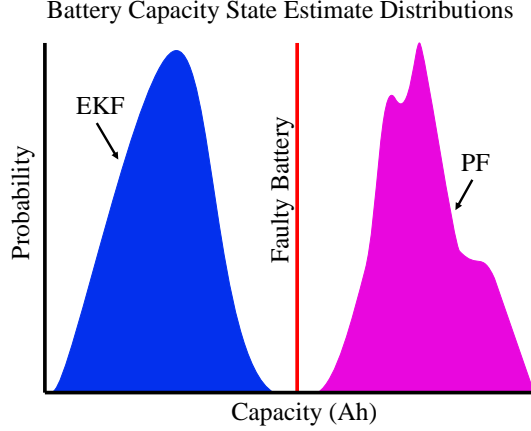
Figure 3.2 Disjoint sets for Dempster Shafer Fusion

extended framework, the degree of trust attributed to a particular belief function is defined as $1 - \alpha_i$, where $0 \leq \alpha_i \leq 1$ and i is the belief function associated with a particular belief measure.

$$
\begin{aligned}
Bel^{\alpha_i}(A) &= (1 - \alpha_i) \cdot Bel(A) \\
\overline{Bel}(A) &= \frac{1}{n} \left(Bel^{\alpha_1}(A) + \ldots + Bel^{\alpha_n}(A) \right)
\end{aligned}
\tag{3.23}
$$

where:

$Bel^{\alpha_i}(A)$ is the discounted belief function

$\overline{Bel}(A)$ is the averaged discounted belief function

This discounting technique has been used to formulate another method for assessing the reliability of two sources, which is explained further in section 4.2.1.

3.4   UNCERTAINTY REPRESENTATION

In the previous section, the accurate representation of uncertainty is identified as a critical step to the proper application of DST. A thorough overview of uncertainty representation is presented in [44]. Uncertainty can be separated into *epistemic* and *aleatory* uncertainty. Aleatory uncertainty describes the natural, unpredictable, and irreducible variation within a system. Expert knowledge can likely provide

16

an estimated magnitude for this uncertainty, but will not reduce it. These are commonly representated by probability distributions. Whereas, epistemic uncertainty is a result of incomplete information about a system, its surrounding environment, or the modeling process. Insufficient experimental data or unmodeled, complex physical dynamics are examples of epistemic uncertainty. This type of uncertainty is able to be properly managed. Without sufficiently identifying and modeling these two categories of uncertainty within an engineered system, this is propagated throughout the model. This unmodeled uncertainty will yield misleading results. The DST framework is uniquely able to accomodate and combine both epistemic and aleatory uncertainty. As uncertainty representation is inherently subjective, it is important that the designer has sufficient knowledge to distinguish between the different uncertainty modes, which can involve both qualitative and quantitative analysis.

3.5 Evaluation Metrics

Different evaluation methods are needed for diagnostics and prognostics. In this section are presented the different categories of metrics used to validate our algorithms.

3.5.1 Aging Detection Metrics

The primary goal of fault detection is the early detection of system faults. This is crucial since the detection of a fault triggers the prognostic algorithm to begin making predictions. In [33], the TTF metric was used for evaluation. This metric demonstrates how early the detection algorithm indicates a fault in the system. A good result is measured by the algorithm which makes earliest fault declaration.

$$TTF = EoL - k_D \tag{3.24}$$
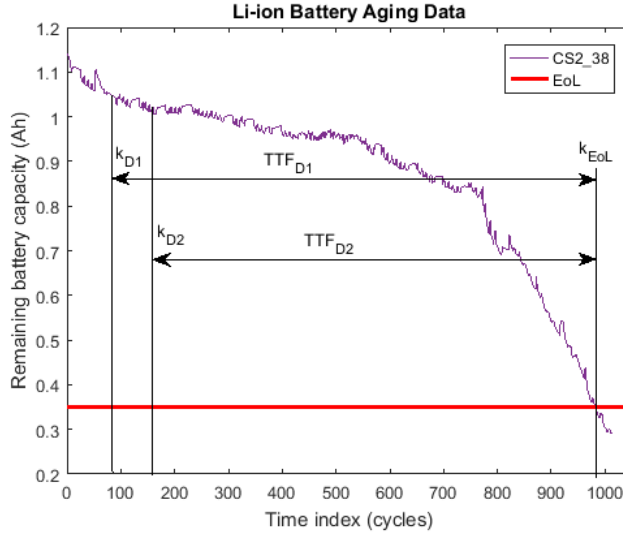
Figure 3.3   The concept of time-to-failure (TTF).

where k_D is the time index at which the fault is detected by diagnostic system. Figure 3.3 illustrates this. Other metrics include sensitivity, selectivity, area under the receiver operating characteristic (ROC) curve, and others mentioned in [45, 46]. As this work is primarily focused on enhanced prognostics, we limit our diagnostic metrics to the earliest TTF generated by each algorithm.

3.5.2   PROGNOSTIC METRICS

Saxena, et al. introduced several metrics for anlayzing the performance of prognostic systems [47], and provided further clarifications for using these metrics in [48]. The concepts presented are successive tests providing quantitative prediction quality. α-λ performance describes whether a prediction falls within specified limits at certain times of the life of the failing system. By requiring the prediction to remain in a specified cone of accuracy, this metric provides a strict requirement for the prognostic algorithm. In this implementation, we define α-λ *accuracy* as follows: $\alpha \times 100\%$ of the ground truth, or baseline, RUL at specific time instance, k_λ, which is a time-step between the first prediction, k_P, and the actual failure, *EoL*. For instance, a choice of

18

$\alpha = 0.2$ and $\lambda = 0.5$ would test the prognostic algorithm for 20% accuracy halfway to EoL after fault detection. This metric can be used to validate both accuracy and precision performance. This concept is further developed through the use of a β criterion, as shown in Eq. (3.26). This helps account for the prediction uncertainty, which is a key factor in this work. The β criterion is defined as the total probability of RUL predictions being within α bounds at time k. Figure 3.4 shows an example of α-λ accuracy with β criterion.

$$(1 - \alpha) \cdot r_*(k) \leq r^l(k_\lambda) \leq (1 + \alpha) \cdot r_*(k) \tag{3.25}$$

where:

l is the lth UUT (i.e. Li-ion battery)

α is an accuracy modifier

λ is a window modifier

$k_\lambda = k_P + \lambda(EoL - k_P)$.

$$\pi[r^l(k)]\Big|_{\alpha^-}^{\alpha^+} \geq \beta$$
$$\alpha^+ = r_*(k) + \alpha \cdot EoL \tag{3.26}$$
$$\alpha^- = r_*(k) - \alpha \cdot EoL$$

where:

β is total probability in [0,1]

$r^l(k)$ is RUL prediction at time k

$r_*(k)$ is baseline RUL prediction at time k.

The output of the metric is binary (Yes or No), stating whether the algorithm meets the requirement within a specific window. The Relative Accuracy (RA) metrics provide further means of quantitative comparison, building upon the α-λ output. RA measures the tracking (above or below the baseline) that an alogorithm performs for the chosen λ set. A RA result in the neighborhood of 1 represent a perfect score, which is interpretted to mean that the predictions perfectly tracked the baseline for a
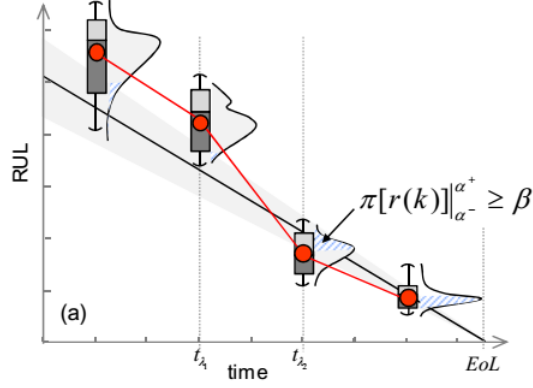
Figure 3.4   The concept of α-λ accuracy [48].

specific λ. Values above or below 1 indicate late or early estimates, respectively. RA only uses the expected value of the RUL prediction at k_λ, so it is used in addition to the above α-λ metric with β criterion.

Cumulative RA (CRA) demonstrates the change in accuracy over time, in which predictions made closer to k_{EoL} are weighted higher than those made closer to k_P. A score close to 1 for CRA represents perfect tracking over the entire λ set. RA and CRA only use the expected value of the RUL prediction at k_λ, so they are used in addition to the above α-λ metric with β criterion.

$$RA_\lambda^l = 1 - \frac{|r_*(k_\lambda) - r^l(k_\lambda)|}{r_*(k_\lambda)} \tag{3.27}$$

$$CRA_\lambda^l = \frac{1}{|\ell_\lambda|} \sum_{i=1}^{\ell_\lambda} w(r^l(i)) RA_\lambda^l \tag{3.28}$$

where:

$w(r^l)$ is a weight factor as a function of RUL at all time indices

ℓ_λ is the set of all time indices before k_λ when a prediction is made

$|\ell_\lambda|$ is the cardinality of the set.

20

CHAPTER 4

APPLICATION WITH LITHIUM-ION BATTERIES

In this section, the proposed approach will be demonstrated in a case study of the capacity degradation of Li-ion batteries. The battery is a safety-critical component that provides power to system functions including command, control, communications, computers, and intelligence. Li-ion batteries are widely used due to the advantages in higher energy density, longer cycle life, no memory effect, and lower weight [49]. Since the life and state of the batteries are not directly measurable, state estimation techniques play an important role in estimating the battery state-of-health and state-of-charge.

In this implementation, the state-of-health of Li-ion batteries with rated capacity of 1.1 Ah are used to verify the proposed approach. The charge-discharge cycle of the battery is conducted with the Arbin BT2000 system under room temperature at a discharge current of 1.1 A. The charging and discharging of the battery are halted at the given cutoff voltage. The capacity degradation curve versus charge-discharge cycle is obtained by Coulomb counting. Figure 4.1 shows the battery aging features for 4 Li-ion battery UUT, denoted as CS2_35 to CS2_38. The EoL of the Li-ion batteries is chosen to be 0.35 Ah from the data.

4.1 STATE ESTIMATION IMPLEMENTATION

For each state estimation technique, a model is develped for use in fault diagnostics and prognostics (FDP). The diagnostic models are configured for one-step-ahead predictions, which allows us to use these models in a recursive architecture for
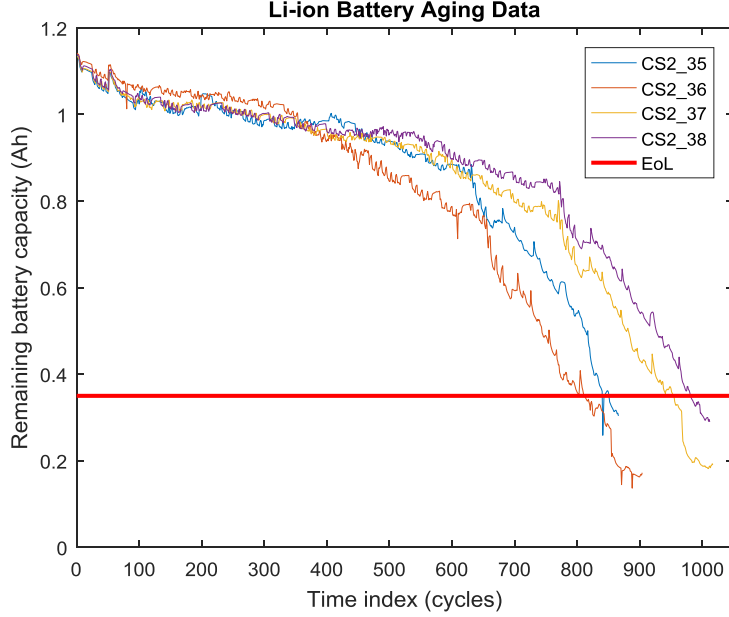
Figure 4.1 Data from run-to-failure test with four Li-ion batteries.

prognostic estimation. The battery is flagged as "aged" once the state estimate is below the detection threshold (1.03 Ah). This threshold is calculated using the first 10% of the values as a baseline. There is slight debouncing added to the threshhold to reduce false alarms. Once the Li-ion battery aging is detected, prognosis algorithm begin generating RUL pdfs in the methods described below.

4.1.1 EKF FDP IMPLEMENTATION

The battery capacity model for EKF is modified from [50] is defined as:

$$C(k+1) = C(k) - p_1 \cdot (p_2 + p_3 \cdot k + p_4 \cdot k^2) \tag{4.1}$$

where C is battery capacity, k is the time index given by cycle number, and $p = [1 \times 10^{-5}, 3.8 \times 10^{-5}, 45, 0.02]$ are parameters. The Jacobian is then calculated for each iteration of new data. As each new data point becomes available, it is analyzed using the EKF. The covariance parameters Q in Eq. (3.6) and R in Eq. (3.8) are

22
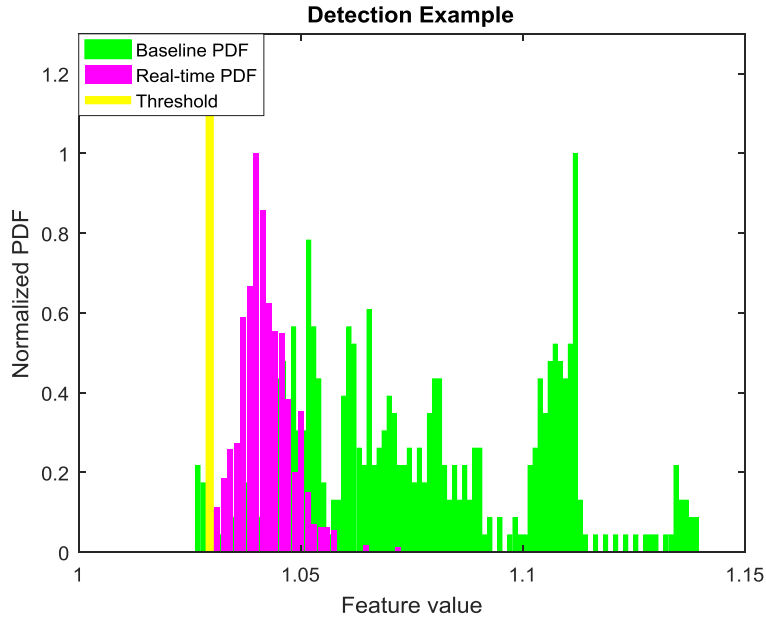
Figure 4.2   Detection is performed by comparing the baseline pdf (healthy battery) and the real-time pdf (based on model and measurement). The threshold is determined by the probability of false alarm. This figure shows an example of particle filter.

used to adjust the dependence of the state estimate upon the model or upon the measurements.

Diagnosis

State estimate pdfs are calculated using the EKF linearized mean and the noise covariances to calculate the spread of the estimate. This pdf is then compared to the detection threshold, as illustrated in Fig. 4.2. Detection is performed by integrating from $-\infty$ to the threshold (for a decreasing fault mode like degradation of battery capacity) or from the threshold to ∞ (for an increasing fault model, such as a crack growing on a component). Once the *probability of detection* is greater than or equal to a threshold, says 90%, the system flags a fault.

Figure 4.3   The fault progression from EKF over time and the generation of RUL pdfs from state estimate, or "damage", pdfs with Gaussian distributions. Uncertainty grows in prognosis since there is no correction step.

Prognosis

Once prognosis is triggered, current state estimate is projected into the future using the model in Eq. (4.1). Figure 4.3 illustrates the process by which state estimate pdfs are converted to TTF or RUL distributions. The TTF is estimated using a Gaussian distribution.

$$CDF_{TTF}(k) = \int\limits_{-\infty}^{F_f} f(x_k | \mu_k, \sigma_k^2) dx \qquad (4.2)$$

As the state estimate crosses the EoL threshold, F_f, a cumulative distribution function (cdf) is generated. Then the pdf of TTF can be calculated from the cdf.

4.1.2   PF FDP Implementation

The battery capacity model for PF is developed from empirical data, and is defined as:

$$C(k+1) = C(k) - p_1 \cdot e^{-p_2 \cdot C(k)} \cdot u(k) \qquad (4.3)$$

24

where C is battery capacity, k is the time index given by cycle number, $p = [92.5 \times 10^{-4}, 2.9]$ are parameters, u is an unknown state, and ω is model noise. The unknown state, u is used to represent dynamics not quantified by the model.

Diagnosis

The PF algorithm uses the model above and performs a one-step-ahead state estimate. The following model for detection is augmented from the fault dynamic model in Eq. (4.3).

$$
\begin{bmatrix} x_{d,1}(k+1) \\ x_{d,2}(k+1) \end{bmatrix} = f_b\left(\begin{bmatrix} x_{d,1}(k) \\ x_{d,2}(k) \end{bmatrix} + n(k) \right)
$$

$$
x_c(k+1) = [x_c(k) - C(k)] \cdot x_{d,2}(k) + \omega k
$$

$$
y(k) = x_c(k) + v(k)
$$

$$
\text{where, } f_b = \begin{cases} [1 \quad 0]^T, \ \textit{if } \left\| x - [1 \quad 0]^T \right\| \leq \left\| x - [0 \quad 1]^T \right\| \\ [0 \quad 1]^T, \ \textit{else} \end{cases}
$$

(4.4)

is a nonlinear mapping, $x_{d,1}$ and $x_{d,2}$ are Boolean states that indicate normal and faulty conditions, respectively, $y(k)$ is the battery capacity from Coulomb counting, $\omega(k)$ and $v(k)$ are noise signals, and $n(k)$ is i.i.d. uniform white noise. When a fault is detected, $x_{d,2} = 1$. The initial condition is given by

$$
\begin{bmatrix} x_{d,1}(0) & x_{d,2}(0) & x_c(0) \end{bmatrix} = [1 \quad 0 \quad 0],
$$

where $x_c(0)$ is the initial battery capacity. With this model, a state estimate pdf is calculated after SIR has been performed to provide the correct weighting. As detailed in section 4.1.1, the detection algorithm compares this pdf to the detection threshold and computes the probability of detection.

Prognosis

Similar to EKF prognosis, once prognosis is triggered, the particles in Eq. (3.15) are projected into the future using the model in Eq. (4.3). Figure 4.4 illustrates how the cdf is quantified using particles. The cdf is calculated by summing the weighted
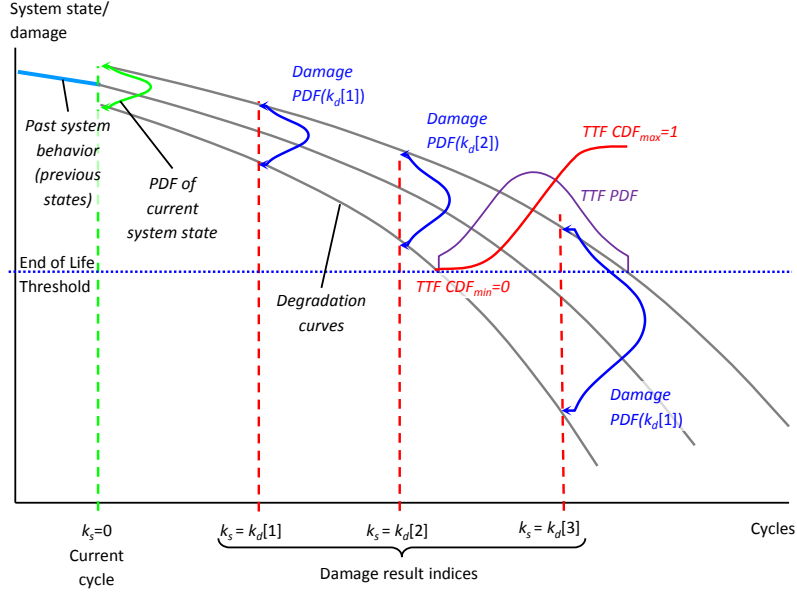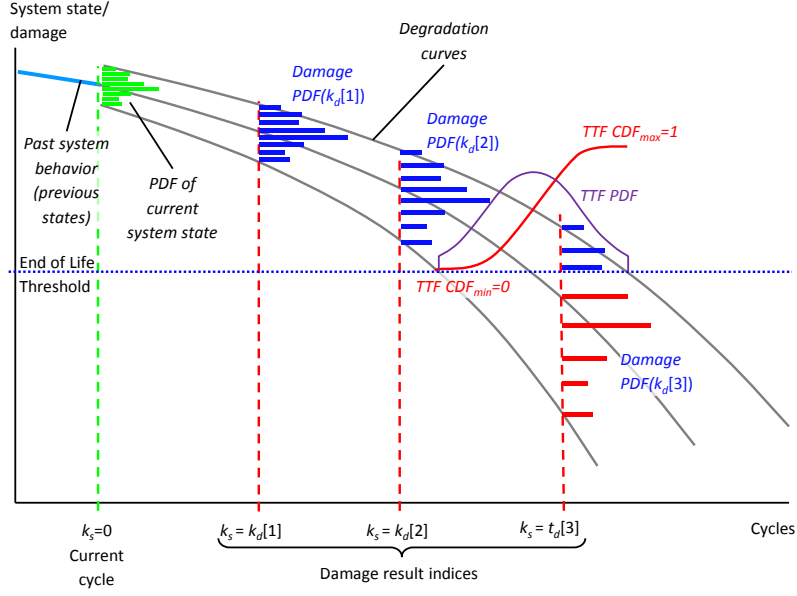
Figure 4.4   The fault progression from PF over time and the generation of RUL pdfs from state estimate, or "damage", pdfs using particles. Uncertainty grows in prognosis since there is no correction step.

particles less than the EoL damage threshold, F_f.

$$CDF_{TTF}(k) = \sum_{i=1}^{N} w_k^{(i)} p\left(failure|x_k^{(i)} < F_f\right) \qquad (4.5)$$

4.2   DATA FUSION

4.2.1   UNCERTAINTY QUANTIFICATION

In designing the uncertainty representation, the dataset including all of the Li-ion battery trajectories over time are investigated. Figure 4.5 shows how aleatory and epistemic uncertainty are represented separately. In this case, *aleatory uncertainty* is evidenced by the random noise in the battery capacity. In our implementation below, EKF and PF have "noise terms", which can be tuned to account for this uncertainty category. During online execution, the prediction variance changes for each cycle.

26

To quantify this uncertainty, Eq. (4.6) is derived. The *spread, S,* of the function is represented by $2 \cdot \sigma^2$, where σ^2 is the variance. If either of the sources exceeds the spread limit, S_{max}, its contribution to the DST combination is ignored. S_{max} is defined as 0.3 Ah for battery capacity state in diagnosis, and 300 cycles for battery EoL in prognosis. The aleatory uncertainty, U_{al}, is represented as

$$U_{al}(k) = \frac{S}{S_{max}} \tag{4.6}$$

Although our models include an unknown state to account for the variety of trajectories, they do not capture all possible variation in trajectory. This unaccounted-for variation in trajectory is classified as *epistemic uncertainty.* Beginning at cycle 400, epistemic uncertainty appears to increase with time. This uncertainty is quantified in our implementation as a time-varying function, Eq. (4.7), given as

$$U_{epi}(k) = (1 - U_{al,k}) \cdot \frac{\epsilon}{1 + e^{-\gamma \cdot (k - k_{off})}} \tag{4.7}$$

where:

ϵ is the maximum uncertainty, $[0, 1]$

γ is the rate-of-change in uncertainty, $[0, 1]$

k_{off} is the offset cycle at which U_{epi} reaches $\frac{\epsilon}{2}$

Equation (4.7) indicates that the uncertainty in a given estimator grows over time, but does not increase beyond a designated maximum. The modified sigmoid function provides a nice framework to represent bounded uncertainty with a growth rate that varies with charge-discharge cycle. For $\gamma = 0$, the epistemic uncertainty is assumed to be constant for all cycles. Since uncertainties must be independent from one another (as required by the DST framework, the general uncertainty function is modified for each state predictor, depending upon the experimental performance of each state predictor at specific instances, Fig. 4.6, which represents experimental testing. EKF performs more stable state estimates and RUL predictions in the first 400 cycles.
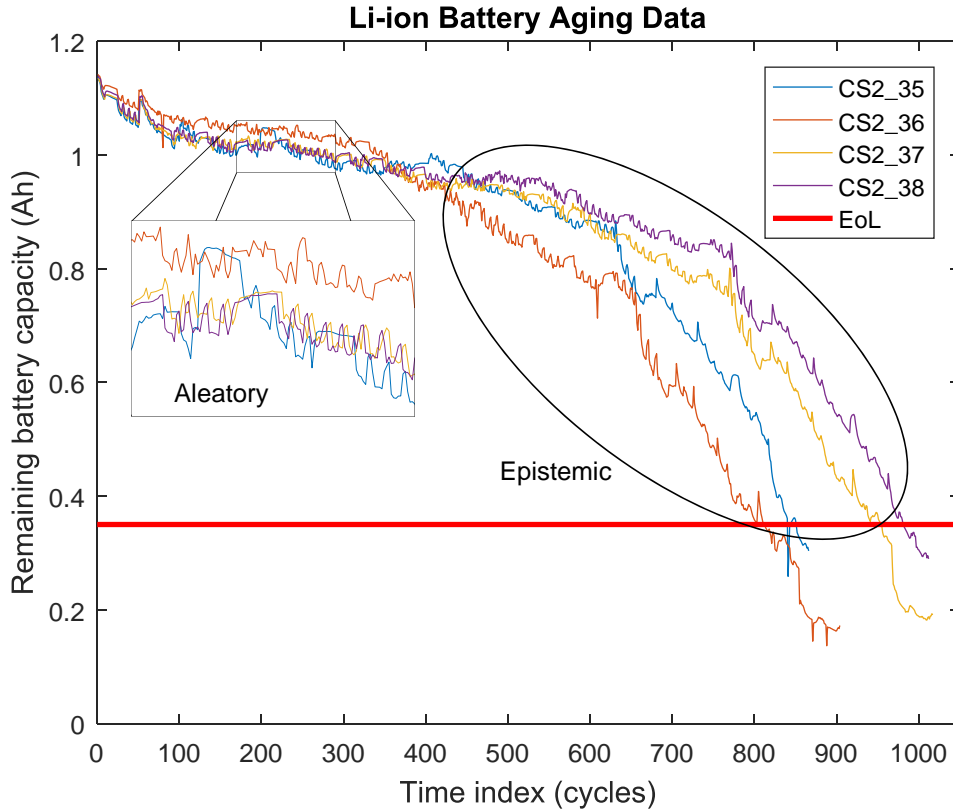
Figure 4.5   Aleatory and epistemic uncertainty represented for Li-ion battery.

However, as the current cycle k approaches the failure threshold k_{EoL}, both PF and EKF perform with similar accuracy. This epistemic uncertainty representation can be improved by performing further experimentation on more Li-ion battery data.

4.2.2   MASS SELECTION FOR HEALTHY AND FAULTY BATTERY

Once the uncertainty is properly accounted for, the remaining two states are considered. The bba for the *faulty* state is assigned as shown in Eq. (4.8) for diagnosis and in Eq. (4.9) for prognosis:

$$m_f(k) = p(failure|x_k < \eta) \cdot (1 - U_{al,k} - U_{epi,k}) \tag{4.8}$$

$$m_f(k) = p(failure|x_k < \xi) \cdot (1 - U_{al,k} - U_{epi,k}) \tag{4.9}$$

28
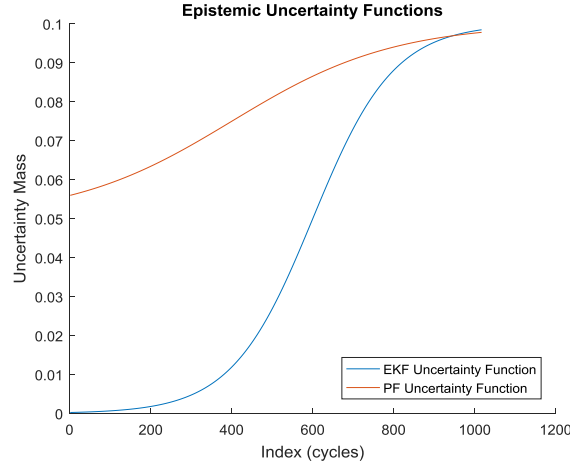
Figure 4.6 Unmodeled uncertainty functions for each RUL prediction alogrithm.

where η is the fault detection threshold, ξ is the failure threshold when the Li-ion battery has reached EoL, and $p(\cdot)$ is a probablity function. The healthy state bba is simply $m_h(k) = 1 - (U_{al,k} + U_{epi,k} + m_{f,k})$, which satisfies the requirement in Eq. (3.19) for the sum of the bba's of all sets be equal to 1.

4.2.3   Combination of Masses

Similar to the example described in section 3.3, Table 4.1 shows the developed combination table using the bba's for the four states developed in the above sections. The green color box area represents the contradictory evidence (i.e. where EKF and PF estimate directly opposing results for the two primary hypotheses: healthy or faulty battery state). The purple color box, $m(F)$, contains the bba combinations where EKF and PF agree with one another. Agreement is quantified in two ways:

1. EKF and PF both *believe* that the battery is faulty (i.e. $m_1(\mu_2) \cdot m_2(\mu_2)$)

2. Either EKF or PF believes the battery is faulty and the other has a degree of uncertainty (e.g. $m_1(\mu_2) \cdot m_2(\mu_3)$).

29

The combined uncertainty is represented by the cyan color box, $m(U)$. Equation (4.10) is the application-specific DST combination for each prediction cycle. Observations of *faulty* states have been combined with each of the *uncertain* states in this architecture. The separation of uncertainty into separate categories allows for interesting results. For instance, even though the prediction spread, described by aleatory uncertainty, U_{al} in Eq. (4.6), and μ_3 in Table 4.1, tends to decrease for both EKF and PF as the current cycle k approaches k_{EoL}, it is possible for EKF and PF to deviate significantly from one another. With the addition of the epistemic uncertainty of modeling error, described by U_{epi} in Eq. (4.7), and μ_4 in Table 4.1, DST can compensate its fusion using the experimental performance of EKF and PF. This also mitigates the problem of disjointed sets. The DST algorithm computes Eq. (4.10) for each cycle.

$$
\begin{aligned}
m(F) =& m(\mu_2){\cdot}m(\mu_2)+m(\mu_2){\cdot}m(\mu_3) \\
&+m(\mu_2){\cdot}m(\mu_4) \\
m(U) =& m(\mu_3){\cdot}m(\mu_3)+m(\mu_3){\cdot}m(\mu_4) \\
&+m(\mu_4){\cdot}m(\mu_4) \\
P_F(k) =& \frac{\sum m(F)}{1-\sum m(\mu_1)\cdot m(\mu_2)} \\
P_U(k) =& \frac{\sum m(U)}{1-\sum m(\mu_1)\cdot m(\mu_2)}
\end{aligned}
\tag{4.10}
$$

where P_F is the belief that a battery fault is detected (diagnosis) or the belief that the battery capacity has degraded to the EoL (prognosis), and P_U is the belief of uncertainty. For diagnosis, P_F is used directly to assess whether the battery capacity is sufficiently degraded to trigger prognosis.

For each cycle of prognosis, Eq. (4.10) is calculated recursively until k reaches k_{EoL}. These results produce a cdf, as shown in Fig. 4.7. Notice that the cdf never reaches "1". This is representative of the fundamental difference between probabilities and bba's. Probability cdfs have unique values for the entire range [0,1], but this does

Table 4.1 The combination of different states within DST framework. m_1 and m_2 represent mass functions for EKF and PF, respectively. μ_1, μ_2, μ_3, μ_4 indciate healthy state, faulty state, aleatory uncertainty, and epistemic uncertainty, respectively.

			PF			
			Healthy	*Faulty*	*Uncertainty$_{al}$*	*Uncertainty$_{epi}$*
			$m_2(\mu_1)$	$m_2(\mu_2)$	$m_2(\mu_3)$	$m_2(\mu_4)$
EKF	*Healthy*	$m_1(\mu_1)$	$m_1(\mu_1)\cdot m_2(\mu_1)$	$m_1(\mu_1)\cdot m_2(\mu_2)$	$m_1(\mu_1)\cdot m_2(\mu_3)$	$m_1(\mu_1)\cdot m_2(\mu_4)$
	Faulty	$m_1(\mu_2)$	$m_1(\mu_2)\cdot m_2(\mu_1)$	$m_1(\mu_2)\cdot m_2(\mu_2)$	$m_1(\mu_2)\cdot m_2(\mu_3)$	$m_1(\mu_2)\cdot m_2(\mu_4)$
	Uncertainty$_{al}$	$m_1(\mu_3)$	$m_1(\mu_3)\cdot m_2(\mu_1)$	$m_1(\mu_3)\cdot m_2(\mu_2)$	$m_1(\mu_3)\cdot m_2(\mu_3)$	$m_1(\mu_3)\cdot m_2(\mu_4)$
	Uncertainty$_{epi}$	$m_1(\mu_4)$	$m_1(\mu_4)\cdot m_2(\mu_1)$	$m_1(\mu_4)\cdot m_2(\mu_2)$	$m_1(\mu_4)\cdot m_2(\mu_3)$	$m_1(\mu_4)\cdot m_2(\mu_4)$

not apply to bba's. Because of the uncertainty quantification, this belief cdf will never reach one. The belief density function (bdf) is then derived from the belief cdf. In order to compare the results from DST to the pdfs generated by the EKF and PF algorithms in prognosis, the bdf is normalized with its maximum value such that the integral over the range is equal to one, similar to a pdf. Also shown in Fig. 4.7 is the uncertainty, P_U. The uncertainty increases about the combination point, which in this application is the EoL, while elsewhere, the uncertainty is flat. This is expected because at the point of combination the normalization denominator varies as EKF and PF RUL trajectories cross the EoL threshold. Prior to k_P, the uncertainty is assumed to be *zero*, since the measurements have already been collected.
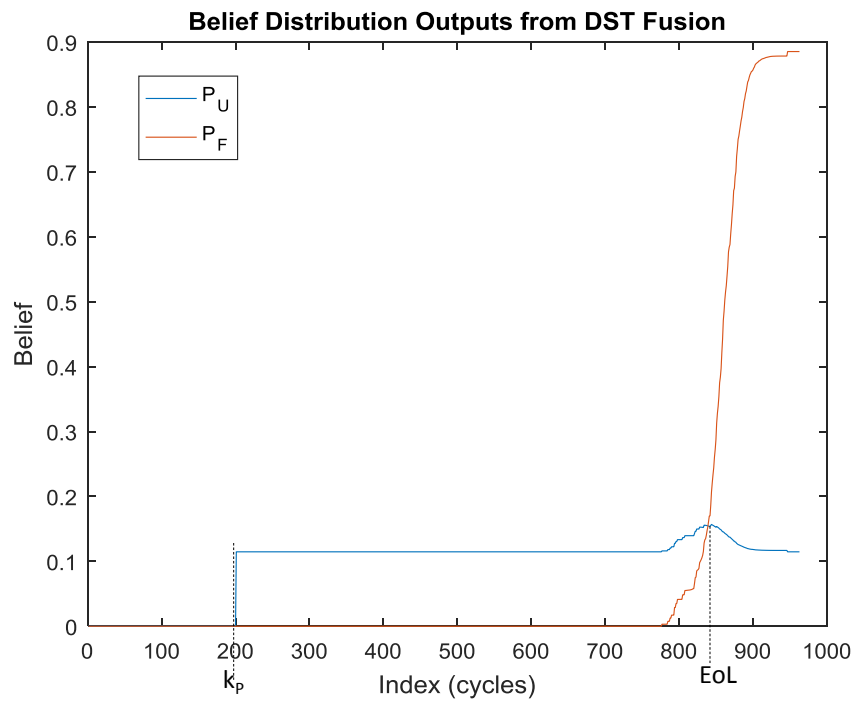
Figure 4.7   The graph depicts the belief distributions generated by DST fusion for prognosis. P_U is the belief uncertainty and P_F is the belief that the battery has reached EoL.

CHAPTER 5

DISCUSSION OF RESULTS

5.1 FAULT DETECTION RESULTS

Each algorithm calculates change in *probability of failure* (PoF) over time. Figure 5.1 shows the PoF after incorporating each algorithm's uncertainty into its PoF. The PF provides earlier indication of fault than EKF, but due to its larger uncertainty, DST "trusts" EKF more. This normalization is calculated as follows:

$$PoF_{norm} = PoF \cdot (1 - \zeta) \tag{5.1}$$

where ζ is the uncertainty. Using normalized PoF's, DST is the clear leader, as its uncertainty is an order of magnitude lower than that of either PF or EKF, as shown in Tables 5.2 - 5.5. To minimize false alarms, algorithms must detect fault for 3 cycles before a fault is declared and prognosis is triggered. These values are calculated at the point of detection for each algorithm, using a detection threshold of 90%. Even though the inital PoF for EKF and PF are higher initially, they have a higher degree of uncertainty. Table 5.1 shows the resulting TTFs for each battery at the point of detectionfor each algorithm. Even though the margin of detection is is low across the alogorithms, DST demonstrates increased performance over either algorithm on its own. In practice, DST is used to trigger prognosis since it detects a fault earlier than EKF and PF, and with a greater degree of certainty.

Table 5.1   TTF Comparison

Battery	PF	EKF	DST	Longest Window
CS2_35	690	688	694	DST
CS2_36	605	641	657	DST
CS2_37	691	783	793	DST
CS2_38	784	799	814	DST

Table 5.2   PoF and Uncertainty Comparison for CS2_35

Algorithm	PoF (%)	Uncertainty	PoF_{norm} (%)
EKF	96.5	0.058	90.8
PF	100	0.093	90.7
DST	95.7	0.007	95.0

Table 5.3   PoF and Uncertainty Comparison for CS2_36

Algorithm	PoF (%)	Uncertainty	PoF_{norm} (%)
EKF	98.3	0.052	93.2
PF	100	0.088	91.2
DST	92.7	0.007	92.0

Table 5.4   PoF and Uncertainty Comparison for CS2_37

Algorithm	PoF (%)	Uncertainty	PoF_{norm} (%)
EKF	97.3	0.052	92.2
PF	100	0.098	90.2
DST	93.0	0.006	92.3

Table 5.5   PoF and Uncertainty Comparison for CS2_38

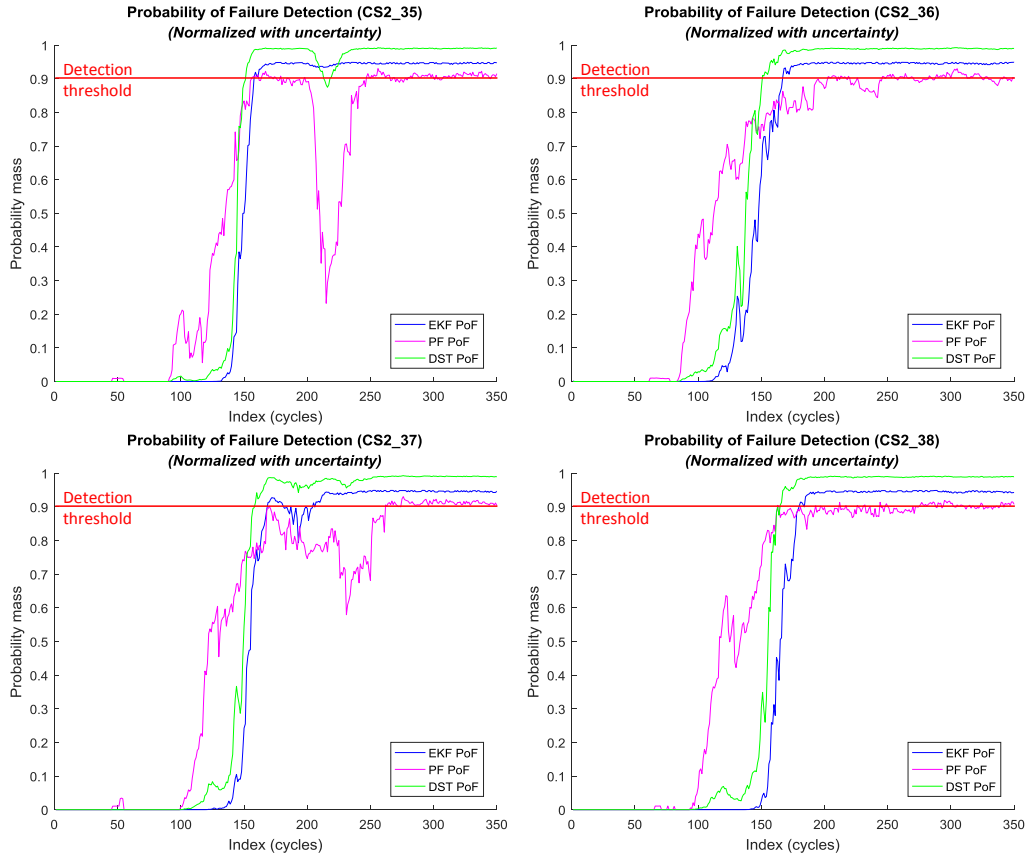| Algorithm	PoF (%)	Uncertainty	PoF_{norm} (%)
EKF	96.2	0.051	91.3
PF	100	0.097	90.3
DST	95.5	0.007	94.8

Figure 5.1   Probability of failure detection results, after normalizing PoF with uncertainty.

5.2   Prognostic Results

Prognosis begins at k_P, the point at which the detection algorithms above signal that the Li-ion battery has aged. RUL is calculated based upon the expected and mean value for PF and EKF, respectively. Figure 5.2 shows how the mean RUL is calculated for each measurement. Performance metrics of 95% confidence intervals (C.I.) are used to calculate the *prediction spread*, $m(\mu_3)$, in Table 4.1.

Each dataset is tested and results from α-λ tests are shown in Table 5.6. This effectively compares how well each algorithm remained within the α-bounds over the entire dataset, while satisfying the β-criterion. The results are shown in %. Results
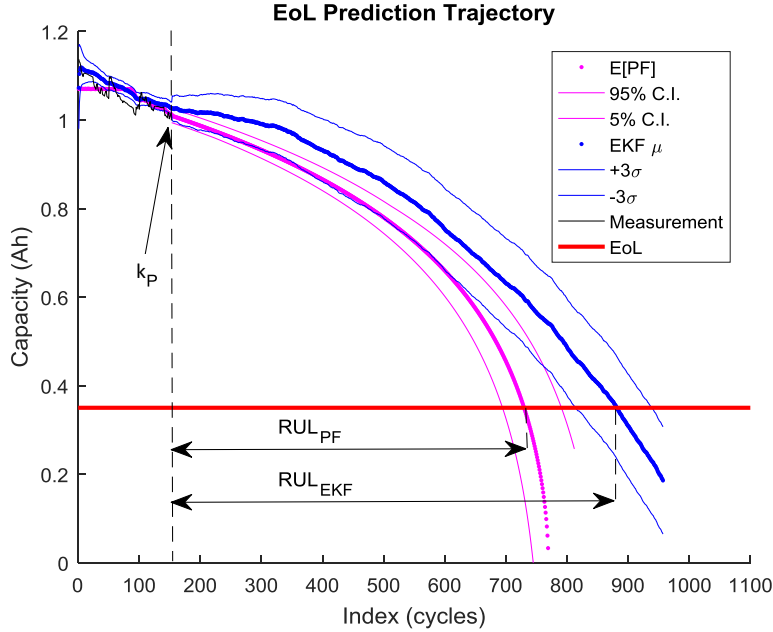
Figure 5.2   The trajectory of PF and EKF prognosis beginning at k_P, shown with confidence bounds.

Table 5.6 α-λ Results with $\alpha = 0.3$ & $\beta = 0.85$

Battery	PF	EKF	DST
CS2_35	36.2%	60.2%	42.0%
CS2_36	84.7%	71.1%	76.3%
CS2_37	89.7%	96.3%	92.3%
CS2_38	83.7%	83.4%	83.1%

for DST lay in between that of EKF and PF for CS2_35 - CS2_37, and performs on par with EKF and PF for CS2_38.

Figures 5.3 - 5.6 show the α-λ plots (with uncertainty bounds shown). DST successfully incoporates the uncertainty within EKF and PF. This is especially evident when EKF and PF RUL predictions are substantially different. Since EKF and PF are separated from one another, the total *uncertainty spread* for DST incorporates these results and produces a wider bdf, even though the expected value is within the specified α limits. To compare results from EKF, PF, and DST for all

batteries, RA and CRA are calculated for every cycle, rather than selecting specific λ's of interest. As shown in these plots, DST primarily tracks the algorithm with the highest demonstrated accuracy, which is the desired performance. For battery CS2_37, this behavior is not observed as prediction are in the neighborhood of the EoL, k_{EoL}. This can be attributed to the epistemic uncertainty functions. Near the EoL, PF produces very narrow confidence bounds, though its mean value may still deviate unacceptably from the baseline, $r_*(k)$. EKF on the other hand does not produce confidence bounds as tight, and due to the assumption of modeling uncertainty made in Fig. 4.6, EKF and PF are treated essentially as equals, with exception to these confidence bounds. Further experimentation may result in improved epistemic uncertainty representation to account for this EoL performance.
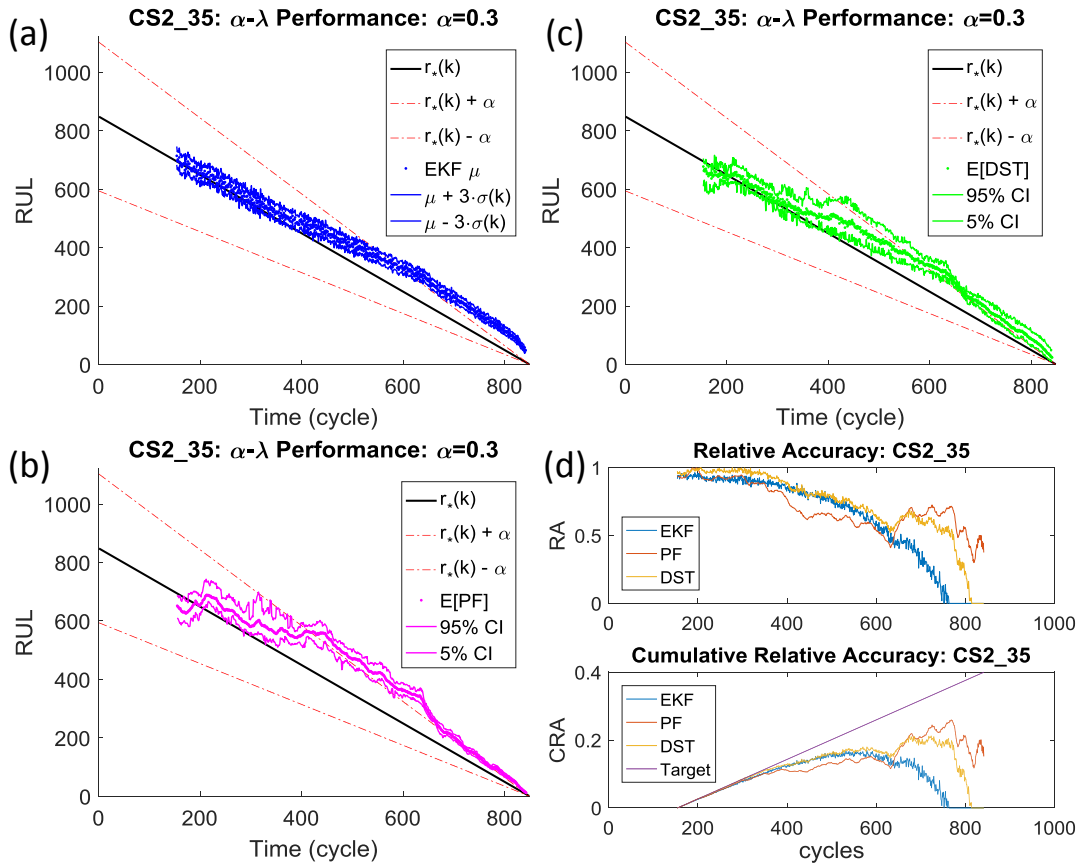
Figure 5.3   Results for CS2_35 Li-ion battery. The upper and lower bounds for each algorithm are shown. (a) EKF α-λ plot, (b) PF α-λ plot, (c) DST α-λ plot, and (d) RA and CRA metrics.
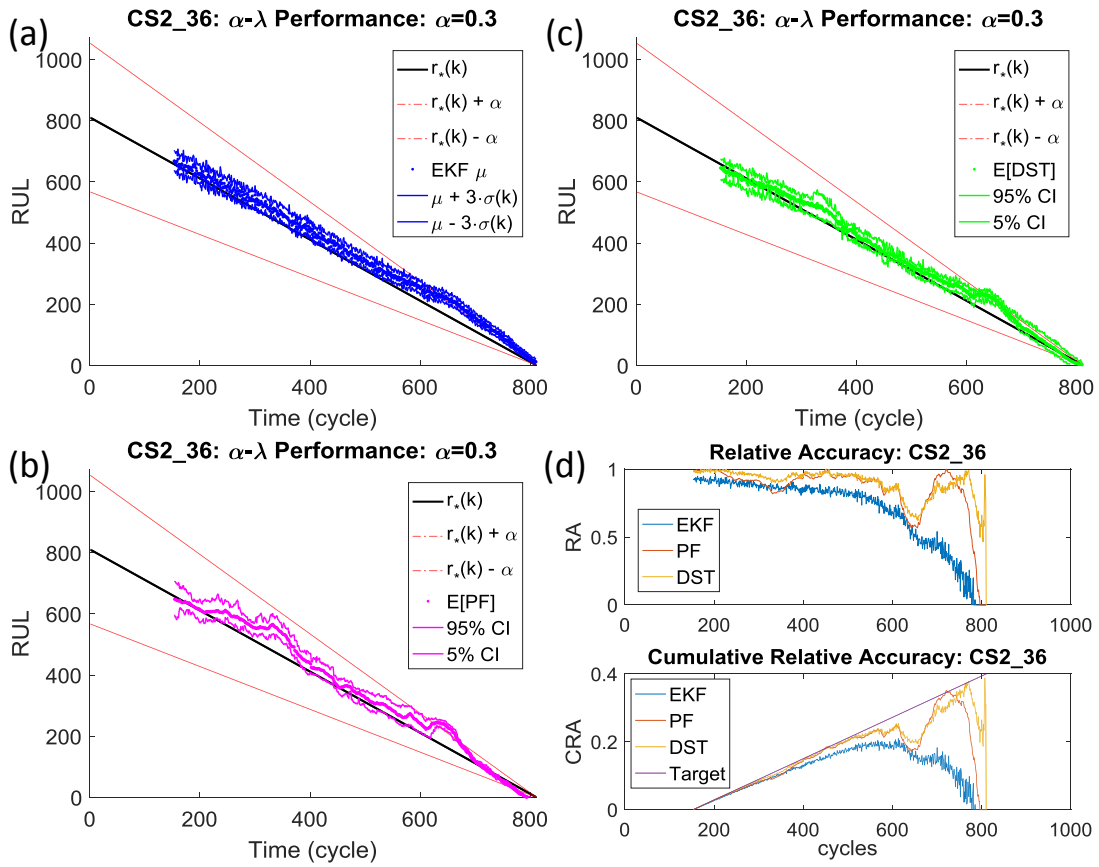
Figure 5.4 Results for CS2_36 Li-ion battery. The upper and lower bounds for each algorithm are shown. (a) EKF α-λ plot, (b) PF α-λ plot, (c) DST α-λ plot, and (d) RA and CRA metrics.
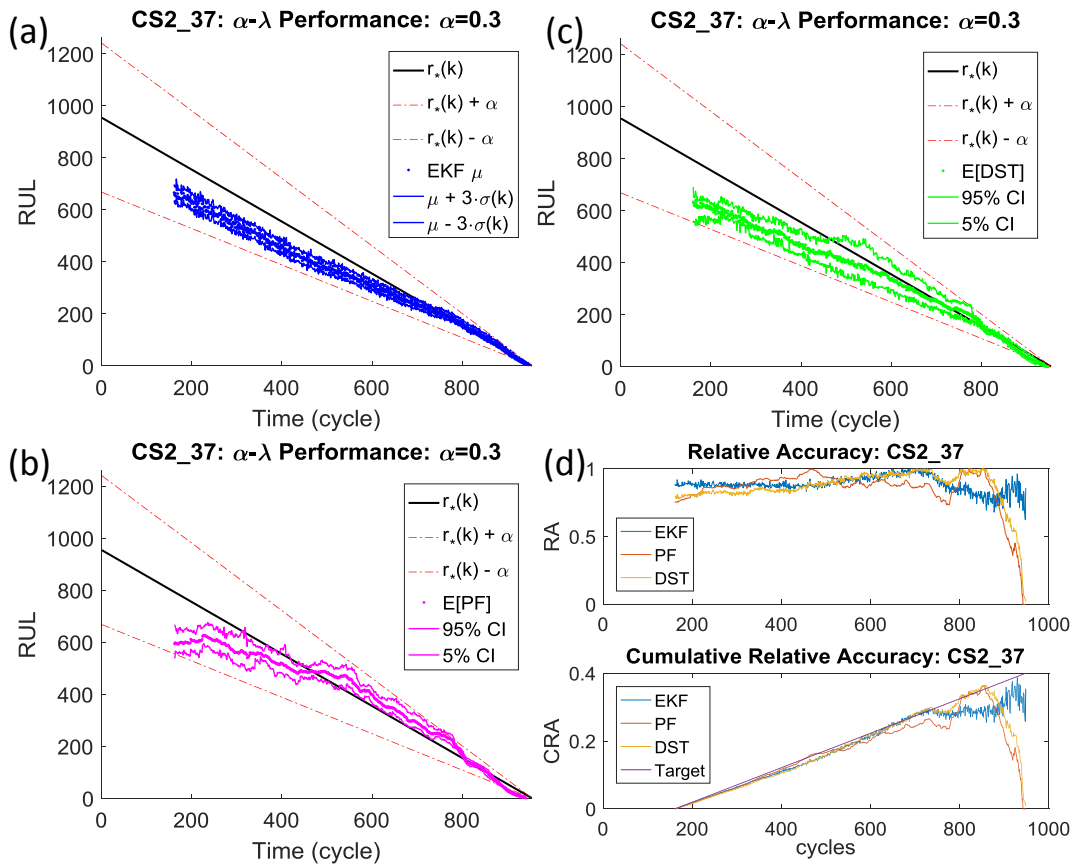
Figure 5.5   Results for CS2_37 Li-ion battery. The upper and lower bounds for each algorithm are shown. (a) EKF α-λ plot, (b) PF α-λ plot, (c) DST α-λ plot, and (d) RA and CRA metrics.
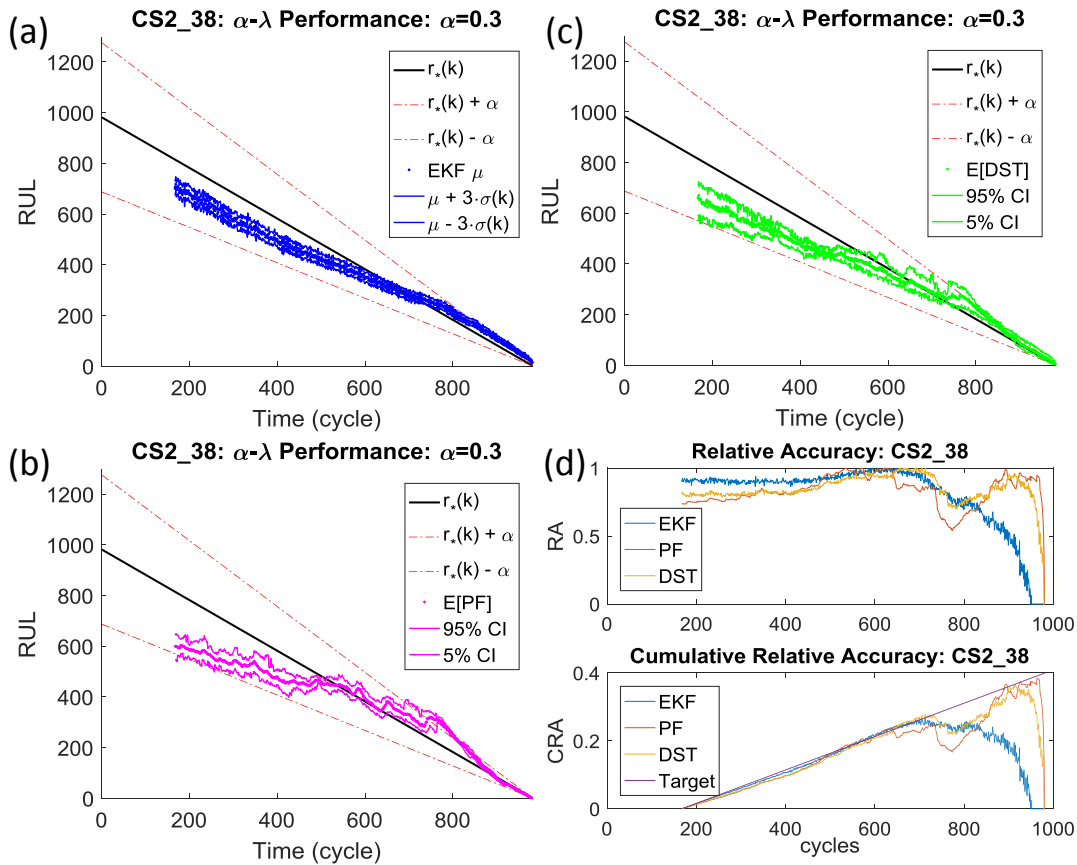
40

Figure 5.6   Results for CS2_38 Li-ion battery. The upper and lower bounds for each algorithm are shown. (a) EKF α-λ plot, (b) PF α-λ plot, (c) DST α-λ plot, and (d) RA and CRA metrics.

CHAPTER 6

CONCLUSION AND FUTURE WORK

6.1 CONCLUSION

DST is a promising method for the fusion of PoF estimates and RUL predictions from
independent sources, while accounting for all uncertainties as shown in the paper.
Uncertainty is explicitly accounted for and combined such that the overall uncertainty
associated with the estimates and predictions is reduced. Uncertainty representation
is paramount to the proper fusion of independent sources. Improper assumptions
about the underlying uncertainty can cause DST to favor one source over another,
as was shown in the α-λ with β-criterion metric. This result could be improved by
either improving the models for EKF and PF, or by further studying the epistemic
uncertainty of both alogrithms and tuning their uncertainty functions. Experimental
testing and simulations can be used to help quantify this uncertainty. DST does show
a reduction in uncertainty in both aging detection and in prognosis. DST produces
the earliest and steepest PoF curve, indicates a high degree of confidence and faster
detection relative to the other algorithms. DST also demonstrates higher precision
in prognosis.

6.2 FUTURE WORK

Representation of the RUL distribution remains a challenge in the DST framework,
since it is using *belief masses* rather than strict probabilities. Another option would
be to consider representing DST belief functions as Dirichlet distributions for both

diagnosis and prognosis. Dirichlet distributions are more natural way of interpretting belief functions from a statistical perspective. Visualizing Dirichlet distributions can be challenging with increasing states, however reserachers have shown promising means of constructing and visualizing multinomal Dirichlet distributions [51]. Another alternative would be to apply the TBM technique introduced in section 1 to Li-ion batteries.

DST has been selected for its inherent flexibility. In this work, two model-based methods using state-observers were fused. It is possible that even better results could be achieved if a data-based method could be fused with a model-based method. Also, the past performance of each could be incoporated into the fusion as a separate state, which could act somewhat like a sliding window. This would likely result in smoother predictions during prognosis.

Bibliography

[1] C. Pillot. "Battery Market Development for Consumer Electronics, Automotive, and Industrial". In: *Batteries 2014*. 2014.

[2] Albemarle. "ALB Lithium Presentation". In: *Goldman Sachs HCID Conference*. 2016.

[3] M. Orchard, P. Hevia-Koch, B. Zhang, and L. Tang. "Risk Measures for Particle-filtering-based State-of-Charge Prognosis in Lithium-Ion Batteries". In: *IEEE Transactions on Industrial Electronics* 60.11 (2013), pp. 5260–526. DOI: 10.1109/TIE.2012.2224079.

[4] B. Zhang, L. Tang, J. DeCastro, M. Roemer, and K. Goebel. "Autonomous Vehicle Battery State-of-Charge Prognostics Enhanced Mission Planning". In: *International Journal of Prognostics and Health Management* 5.2 (2014).

[5] J. Kim and B. Cho. "An innovative approach for characteristic analysis and state-of-health diagnosis for a Li-ion cell based on the discrete wavelet transform". In: *Journal of Power Sources* 260 (2014), 115âĂŞ130.

[6] S. Gadsden and S. Habibi. "Model-based fault detection of a battery system in a hybrid electric vehicle". In: *Proceedings of the 7th IEEE Vehicle Power and Propulsion Conference (VPPC '11)*. 2011.

[7] A. Singh, A. Izadian, and S. Anwar. "Fault Diagnosis of Li-Ion Batteries Using Multiple-Model Adaptive Estimation". In: *39th Annual Conference of the IEEE Industrial Electronics Society*. 2013. DOI: 978-1-4799-0223-1/13.

[8] J. Kim and B. Cho. "A Review on Fault Mechanism and Diagnosis Approach for Li-Ion Batteries". In: *Journal of Nanomaterials* (2015). DOI: 631263.

[9] A. Sidhu, A. Izadian, and S. Anwar. "Adaptive Nonlinear Model-Based Fault Diagnosis of Li-Ion Batteries". In: *IEEE Transactions on Industrial Electronics* 62.2 (2015). DOI: 10.1109/TIE.2014.2336599.

[10] C. Chen, B. Zhang, G. Vachtsevanos, and M. Orchard. "Machine Condition Prediction based on Adaptive Neuro-Fuzzy and High-Order Particle Filtering". In: *IEEE Transactions on Industrial Electronics* 58.9 (2011), pp. 4353–4364. DOI: 10.1109/TIE.2010.2098369.

[11] C. Chen, Brown, D., C. Sconyers, B. Zhang, G. Vachtsevanos, and M. Orchard. "An integrated architecture for fault diagnosis and failure prognosis of complex engineering systems". In: *Expert Systems with Applications* 39.10 (2012), pp. 9031–9040. DOI: 10.1016/j.eswa.2012.02.050.

[12] K. Goebel, B. Saha, A. Saxena, J. R. Celaya, and J. Christophersen. "Prognostics in Battery Health Management". In: *IEEE Instrumentation & Measurement Magazine* 11.4 (2008), pp. 33–40. DOI: 10.1109/MIM.2008.4579269.

[13] G. Box, G. Jenkins, and G. Reinsel, eds. *Time Series Analysis: Forecasting and Control.* Hoboken: John Wiley & Sons, Inc, 2008.

[14] B. Saha, K. Goebel, and J. Christophersen. "Comparison of prognostic algorithms for estimating remaining useful life of batteries". In: *Transactions of the Institute of Measurement and Control* 31.3-4 (2009), pp. 293–308. DOI: 10.1177/0142331208092030.

[15] K. Goebel and P. Bonissone. "Prognostic information fusion for constant load systems". In: *8th International Conference on Information Fusion.* 2005. DOI: 10.1109/ICIF.2005.1592000.

[16] K. Goebel and N. Eklund. "Prognostic Fusion for Uncertainty Reduction". In: *AIAA Infotech@Aerospace 2007 Conference and Exhibit*. 2007. DOI: `10.2514/6.2007-2843`.

[17] S. Cheng and M. Pecht. "A Fusion Prognostics Method for Remaining Useful Life Prediction of Electronic Products". In: *5th Annual IEEE Conference on Automation Science and Engineering*. 2009. DOI: `10.2514/6.2007-2843`.

[18] D. Wang, P. W. Tse, W. Guo, and Q. Miao. "Support vector data description for fusion of multiple health indicators for enhancing gearbox fault diagnosis and prognosis". In: *Measurement Science and Technology* 22.2 (2011).

[19] F. Castanedo. "A Review of Data Fusion Techniques". In: *The Scientific World Journal* 2013.704504 (2013), p. 19. DOI: `10.1155/2013/704504`.

[20] B. Parhami. "Voting: A Paradigm for Adjunction and Data Fusion in Dependable Systems". In: *Dependable Computing Systems* (2005), pp. 87–114.

[21] S. Blank, T. Fűhst, and K. Berns. "A Fuzzy Approach to Low Level Sensor Fusion with Limited System Knowledge". In: *13th Conference on Information Fusion*. 2010.

[22] F. Russo and G. Ramponi. "Fuzzy Methods for Multisensor Data Fusion". In: *IEEE Transactions on Instrumentation and Measurement* 43.2 (1994), pp. 288–294.

[23] D. Koks and S. Challa. *An Introduction to Bayesian and Dempster-Shafer Data Fusion*. Tech. rep. 1436. DSTO Systems Sciences Laboratory, 2003.

[24] J. Carl. "Handbook of Multisensor Data Fusion". In: ed. by D. Hall and J. Llinas. Boca Raton: CRC Press LLC, 2001. Chap. Contrasting Approaches to Combine Evidence, p. 32.

[25] G. Shafer, ed. *A Mathematical Theory of Evidence*. Princeton University Press, 1976.

[26] G. Shafer. "Perspectives on the theory and practice of belief functions". In: *International Journal of Approximate Reasoning* 4.5-6 (1990), pp. 323–362. DOI: `10.1016/0888-613X(90)90012-Q`.

[27] M. Roemer, G. Kacprzynski, and M. Schoeller. "Improved diagnostic and prognostic assessments using health management information fusion". In: *AUTOTESTCON Proceedings, 2001*. 2001. DOI: `10.1109/AUTEST.2001.948984`.

[28] O. Basir, F. Karray, and H. Zhu. "An innovative approach for characteristic analysis and state-of-health diagnosis for a Li-ion cell based on the discrete wavelet transform". In: *IEEE Transactions on Neural Networks* 16.6 (2005), pp. 1513–1530.

[29] A. Jøsang and Z. Elouedi. "Constructing the Pignistic Probability Function in a Context of Uncertainty". In: *Fifth Annual Conference on Uncertainty in Artificial Intelligence*. 1989.

[30] P. Smets and R. Kennes. "The transferable belief model". In: *Artificial intelligence* 66.2 (1994), pp. 191–234.

[31] S. Petit-Renaud and T. Denœux. "Nonparametric regression analysis of uncertain and imprecise data using belief functions". In: *International Journal of Approximate Reasoning* 35.1 (2004), pp. 1–28.

[32] G. Niu and B.-S. Yang. "Dempster-Shafer regression for multi-step-ahead time-series prediction towards data-driven machinery prognosis". In: *Mechanical systems and signal processing* 23.3 (2009), pp. 740–751.

[33] J. Weddington, W. Yan, W. Dou, and B. Zhang. "Battery Capacity Anomaly Detection and Data Fusion". In: *Annual Conference of the Prognostics and Health Management Society*. 2015.

[34] B. Zhang, T. Khawaja, R. Patrick, G. Vachtsevanos, M. Orchard, and A. Saxena. "A novel blind deconvolution de-noising scheme in failure prognosis". In: *Transactions of the Institute of Measurement and Control* 32.1 (2010), pp. 3–30. DOI: `10.1177/0142331209357844`.

[35] B. Zhang, C. Sconyers, C. Byington, R. Patrick, M. Orchard, and G. Vachtsevanos. "A Probabilistic Fault Detection Approach: Application to Bearing Fault Detection". In: *IEEE Transactions on Industrial Electronics* 58.5 (2011), pp. 2011–2018. DOI: `10.1109/TIE.2010.2058072`.

[36] M. Arulampalam, S. Maskell, N. Gordon, and T. Clapp. "A tutorial on particle filters for online nonlinear/non-Gaussian Bayesian tracking". In: *IEEE Transactions on Signal Processing* 50.2 (2002), pp. 174–188. DOI: `10.1109/78.978374`.

[37] E. Auer, W. Luther, G. Rebner, and P. Limbourg. "A verified matlab toolbox for the dempster-shafer theory". In: *Workshop on the Theory of Belief Functions*. 2010.

[38] G. Shafer. "A generalization of Bayesian inference". In: *Journal of the Royal Statistical Society* Series B.30 (1968), pp. 205–247. DOI: `10.1007/978-3-540-44792-4\_4`.

[39] H. Wu, M. Siegel, R. Stiefelhagen, and J. Yang. "Sensor Fusion Using Dempster-Shafer Theory". In: *IEEE Instrumentation and Measurement Technology Conference*. 2002.

[40] K. Sentz and S. Ferson. *Combination of Evidence in Dempster-Shafer Theory*. Tech. rep. 0835. Sandia National Laboratories, 2002.

[41] A. Brodzik and R. Enders. *A case of combination of evidence in the Dempster-Shafer theory inconsistent with evaluation of probabilities*. Tech. rep. 2011. DOI: `arXiv:1107.0082v1`.

[42] L Zadeh. "On the validity of Dempster's rule of combination, Memo M 79/24". In: *Univ. of California, Berkeley* 74 (1979).

[43] G. Shafer and J. Pearl, eds. *Readings in Uncertain Reasoning.* Morgan Kaufmann, 1990.

[44] C. Mozumder. "Robust Design: Uncertainty Representation and Propagation". PhD thesis. Department of Aerospace Engineering, Indian Institute of Technology, Bombay, 2004.

[45] U. Okeh and C. Okoro. "Evaluating Measures of Indicators of Diagnostic Test Performance: Fundamental Meanings and Formulars". In: *J Biomet Biostat* 3.1 (2012). DOI: 10.4172/2155-6180.1000132.

[46] A. Simundic. "Measures of Diagnostic Accuracy: Basic Definitions". In: *EJIFCC* 19.4 (2009), pp. 203–211.

[47] A. Saxena, J. Celaya, B. Saha, S. Saha, and K. Goebel. "Metrics for Evaluating Performance of Prognostic Techniques". In: *International Conference on Prognostics and Health Management (PHM).* 2008.

[48] A. Saxena, J. Celaya, E. Balaban, K. Goebel, B. Saha, S. Saha, and M. Schwabacher. "On Applying the Prognostic Performance Metrics". In: *International Conference on Prognostics and Health Management (PHM).* 2009.

[49] B. Saha and K. Goebel. "Modeling Li-ion Battery Capacity Depletion in a Particle Filtering Framework". In: *Annual Conference of the Prognostics and Health Management Society.* 2009.

[50] W. Yan, B. Zhang, X. Wang, and W. Dou. "Lebesgue Sampling-Based Diagnosis and Prognosis for Lithium-Ion Batteries". In: *IEEE Transactions on Industrial Electronics* 63.3 (2016), pp. 1804 –1812. DOI: 10.1109/TIE.2015.2494529.

[51] A. Jøsang and Z. Elouedi. "Interpreting Belief Functions as Dirichlet Distributions". In: *9th European Conference on Symbolic and Quantitative Approaches to Reasoning with Uncertainty*. 2007.